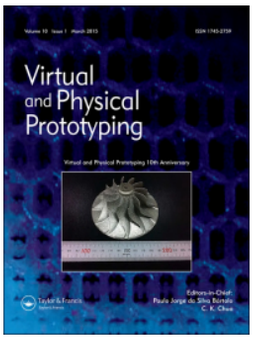

Virtual and Physical Prototyping

ISSN: 1745-2759 (Print) 1745-2767 (Online) Journal homepage: www.tandfonline.com/journals/nvpp20

# A dragonfly-inspired metamaterial device with tunable stiffness and damage-sensitive dynamic response

Kefan Guo , Chong Li , Chen Gong , Yinong Li , Li Cheng & Yang Lu

**To cite this article:** Kefan Guo , Chong Li , Chen Gong , Yinong Li , Li Cheng & Yang Lu (2025) A dragonfly-inspired metamaterial device with tunable stiffness and damage-sensitive dynamic response, Virtual and Physical Prototyping, 20:1, e2567388, DOI: 10.1080/17452759.2025.2567388

**To link to this article:** https://doi.org/10.1080/17452759.2025.2567388



Published online: 06 Oct 2025.

VIRTUAL AND PHYSICAL PROTOTYPING
2025, VOL. 20, NO. 1, e2567388 (13 pages)
https://doi.org/10.1080/17452759.2025.2567388



# A dragonfly-inspired metamaterial device with tunable stiffness and damage-sensitive dynamic response

Kefan Guo[a]*, Chong Li[a]*, Chen Gong[b], Yinong Li[a], Li Cheng[b] and Yang Lu[a,c]

[a]Department of Mechanical Engineering, The University of Hong Kong, Kowloon, People's Republic of China; [b]Department of Mechanical Engineering, The Hong Kong Polytechnic University, Kowloon, People's Republic of China; [c]Materials Innovation Institute for Life Sciences and Energy (MILES), HKU-SIRI, Shenzhen, People's Republic of China

**ABSTRACT**

Architected structures with embedded stimuli-responsive materials offer new opportunities for programmable vibration control. However, preserving robust modal integrity under structural damage, especially in anisotropic systems, remains a fundamental challenge. To address these limitations, we propose a dragonfly-inspired metamaterial device that integrates magnetorheological fluid (MRF), enabling dynamic stiffness modulation and real-time recovery under magnetic fields. Under quasi-static compression in-plane (Z-axis), the application of a 30 mT magnetic field increases structural stiffness by 667% and enhances energy absorption by 4 times. Under dynamic excitation out-of-plane (Y-axis), magnetic fields induce a tunable reduction in effective modal stiffness, enabling reversible, contactless frequency control. When artificial cracks are introduced, the system restores vibrational coherence through magnetic field-induced reconfiguration, effectively compensating for the damage-induced modal shifts. This structural self-healing of vibrational properties demonstrates real-time response without physical intervention. This study establishes a multifunctional, reconfigurable wing architecture with potential applications in smart aerospace structures, structural health monitoring, and adaptive vibration control.

**ARTICLE HISTORY**
Received 9 August 2025
Accepted 23 September 2025

**KEYWORDS**
Bio-inspired metamaterials; magnetorheological fluid; tunable stiffness; damage-adaptive dynamics; self-healing

## 1. Introduction

Architected metamaterial devices or systems with tunable stiffness and integrated multifunctionality have attracted increasing attention as next-generation solutions for intelligent structural design. They have demonstrated potential applications in various fields, particularly in aerospace engineering, vibration-sensitive platforms, and real-time structural health monitoring [1–5]. A key innovation of these systems lies in their ability to embed programmable mechanical behaviour directly into the material's architecture, thus eliminating the reliance on traditional mechanical components [6–10]. While rooted in conventional lightweight lattice structures that enhance mechanical efficiency, energy dissipation, and load-specific stiffness, existing systems remain fundamentally limited by static topologies and are unable to dynamically adapt their behaviour to evolving operational demands or damage conditions, which restricts their applicability in real-world, high-performance scenarios [11–13]. To overcome these limitations, recent research has focused on integrating stimuli-responsive materials into geometrically optimised frameworks, enabling the development of architected systems that combine mechanical efficiency with spatiotemporal reconfigurability [14–18].

In parallel, the field of lattice structure design has established a comprehensive framework for tailoring stiffness, damping, and modal behaviour. Classical beam-based lattices are categorised as stretch-dominated or bending-dominated, with the former ensuring efficient load transfer and the latter enhancing compliance and energy absorption [19]. Beyond periodic and uniform topologies, graded and hierarchical lattices enable spatial modulation of stiffness and defect tolerance [20], while triply periodic minimal surface (TPMS) and shell-like architectures provide smooth stress redistribution and broadband dynamic control [21,22]. The essence of these design strategies lies in exploiting anisotropy, graded density, and hierarchical organisation to

**CONTACT** Yang Lu ylu1@hku.hk Department of Mechanical Engineering, The University of Hong Kong, 518057, Kowloon, People's Republic of China; Materials Innovation Institute for Life Sciences and Energy (MILES), HKU-SIRI, Shenzhen, People's Republic of China
*Kefan Guo and Chong Li contributed equally to this work.
Supplemental data for this article can be accessed online at https://doi.org/10.1080/17452759.2025.2567388.

steer where stiffness and curvature localise within the lattice [23,24]. By directly coupling local deformation pathways to global vibrational modes, such approaches establish the structural basis for achieving defect tolerance and modal coherence in multifunctional metamaterial systems. However, existing studies rarely address dynamic modal control under defect conditions, which is crucial for applications requiring robust performance under operational changes or structural damage.

Among biological structures, dragonfly wings offer a compelling model of mechanical adaptability and multifunctional optimisation [25,26]. Their architecture features hierarchical hexagonal lattices and compliant membranes that work in concert to achieve high stiffness-to-weight ratios, directional damping, and localised damage tolerance [27,28]. These capabilities arise from spatial stiffness gradients, dynamic energy redistribution, and passive modulation of vibrational modes through geometric tailoring [29,30]. Recent biomechanical studies have shown that the decoupling of structural response across different wing regions enables distributed load management and frequency partitioning during flight [25,31,32]. This naturally encoded anisotropy and segmentation of vibration modes provide insights for the design of synthetic systems allowing for programmable stiffness control and spatially resolved vibration tuning [33–36]. The bioinspired lattice structures have emerged as a promising foundation for developing architected metamaterial devices that integrate structural efficiency with adaptive dynamic functionality [37–39]. Nevertheless, most dragonfly-inspired systems have emphasised static load efficiency or passive damping, with limited exploration of direction-dependent, reversible modal tuning under structural defects.

Building on these structural principles and biological inspirations, recent studies have embedded stimuli-responsive media into architected lattices to achieve real-time mechanical tuning [40–42]. Magnetorheological fluid (MRF) is particularly attractive due to its ability to reversibly modulate stiffness and damping under applied magnetic fields. When embedded into a structural framework, the MRF allows programmable and contactless control of mechanical behaviour, supporting functions such as adaptive vibration isolation and tunable resonance [43,44]. Recent work has begun incorporating the MRF into mechanical metamaterial devices to achieve more advanced capabilities, including wave propagation manipulation, dynamic load redistribution, and spatially resolved frequency control [45,46]. While magnetically responsive inclusions have been used to modulate resonant behaviour in architected systems, existing strategies rarely address modal control under distributed structural defects and offer direction-dependent, reversible tuning of vibrational properties via external stimuli [44,47]. This limits their applicability in scenarios where modal coherence is essential and underscores the need for multifunctional systems capable of stiffness adaptation, tunable frequency response, and dynamic recovery under damage. Moreover, existing MRF-integrated metamaterials rarely combine bioinspired lattice principles with defect-tolerant modal recovery, leaving a gap at the intersection of biological anisotropy and magnetically reconfigurable mechanics. In contrast to previous bioinspired studies that primarily emphasised static efficiency or passive damping, and beyond earlier MRF-based metamaterials that focused on uniform stiffness modulation without addressing damage tolerance, existing strategies have yet to realise systems capable of direction-dependent and defect-tolerant modal control.

To address this challenge, we propose a magnetically tunable metamaterial device inspired by the hexagonal lattice structure of dragonfly wings. The design incorporates the MRF into hollow microchannels, allowing for direction-dependent modulation of stiffness and modal behaviour under external magnetic fields. Magnetic activation induces particle chain formation within the channels, resulting in localised stiffness changes without altering global geometry. We first characterise the system under quasi-static compression in-plane, where magnetic activation increases the effective stiffness by 667% and enhances energy absorption by ~4 times. Under dynamic excitation out-of-plane, the applied magnetic field reduces the resonant frequency by lowering the system's effective modal stiffness. Finally, when artificial cracks are introduced, this tunable response constitutes a function-level self-healing mechanism, whereby field-induced microstructural realignment compensates for local stiffness changes and restores disrupted modal frequencies. The process enables on-demand recovery of dynamic performance under structural damage, without the need for physical repair. The proposed design offers a magnetic strategy for programmable vibration control, conducive to applications requiring the preservation of the integrity of modal responses under structural damage, such as morphing aerospace components and integrated health-monitoring systems.

## 2. Materials and method

### 2.1. Dragonfly-inspired metamaterial device structural design

The structural design of the metamaterial device is inspired by the anisotropic mechanical characteristics of dragonfly wings, which arise from the spatial alternation of rigid vein skeletons and compliant membrane

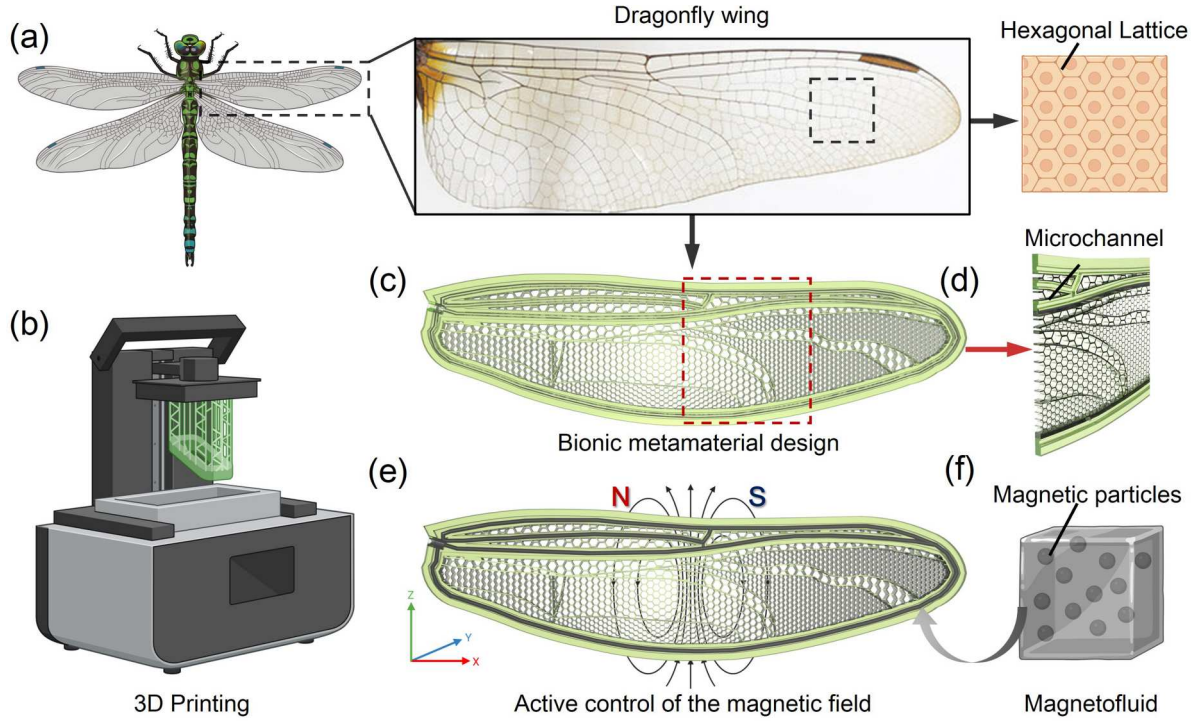


**Figure 1.** Design and fabrication of the bioinspired magnetoactive metamaterial device. (a) Dragonfly wing venation as structural inspiration. (b) 3D printing of the metamaterial device. (c) Hexagonal microlattice with rigid outer frame of metamaterial device. (d) Embedded microchannels for MRF filling. (e) Magnetic field applied perpendicular to the wing plane. (f) MRF composed of $Fe_3O_4$ nanoparticles suspended in oil.

regions. As illustrated in Figure 1a, the hollow, polygonal vein framework encloses soft membrane domains. This composite configuration exhibits distinct directional stiffness depending on the applied loading direction. Bioinspired by the venation layout of dragonfly wings, we construct a lattice-based metamaterial architecture composed of rigid hexagonal units to emulate the mechanical segmentation of natural wings.

As shown in Figure 1c, the device adopts a regular hexagonal microlattice enclosed by a rigid frame, emulating the venation-segmented architecture of dragonfly wings. Quantitative parameters of the fabricated wing are summarised in Supplementary Tables S1–S3. The overall structure measures $131.36 \times 36.48 \times 3.20$ mm ($L \times W \times H$), yielding an aspect ratio of 3.60 and a thickness ratio $H/L = 0.024$. Importantly, despite the varying cell sizes and strut thicknesses, the in-plane relative density remains nearly constant ($\rho^* \approx 0.226$-$0.229$), ensuring mass efficiency while enabling functional segmentation. This architecture is intentionally non-periodic: the lattice is partitioned into large-, medium-, and small-cell regions to keep the in-plane relative density nearly constant while varying the local $t/a$ ratio, thereby redistributing stiffness and modal participation without a mass penalty. In this way, global stiffness, regional modal tuning, and local compliance/crack-tolerance can coexist within a single structure. A comparative overview situating this non-periodic, channelised design among bioinspired and magnetically tunable lattices is provided in Supplementary Table S4.

A venation-mimicking microchannel network is integrated into the perimeter and inner beams. The channels have a circular cross-section of 1.20 mm in diameter and a total centreline length of ≈ 1.08 m, corresponding to an MRF filling volume of ≈ 1.22 mL. This provides sufficient fluid capacity to enable field-driven stiffness modulation, while preserving the modal integrity of the lattice under external loading and crack introduction.

### 2.2. Fabrication and MRF integration

The device is fabricated using a high-resolution LCD-based MSLA printer (Phrozen Sonic Mighty 12 K; Figure 1b). A transparent nylon-based photocurable resin is selected to balance mechanical strength and feature resolution. Printing exposure conditions and build orientation are optimised to minimise residual stresses during support removal, thereby preserving the dimensional precision of embedded microchannels.

After the printing supports are removed, MRF is infused into the internal microchannels through a

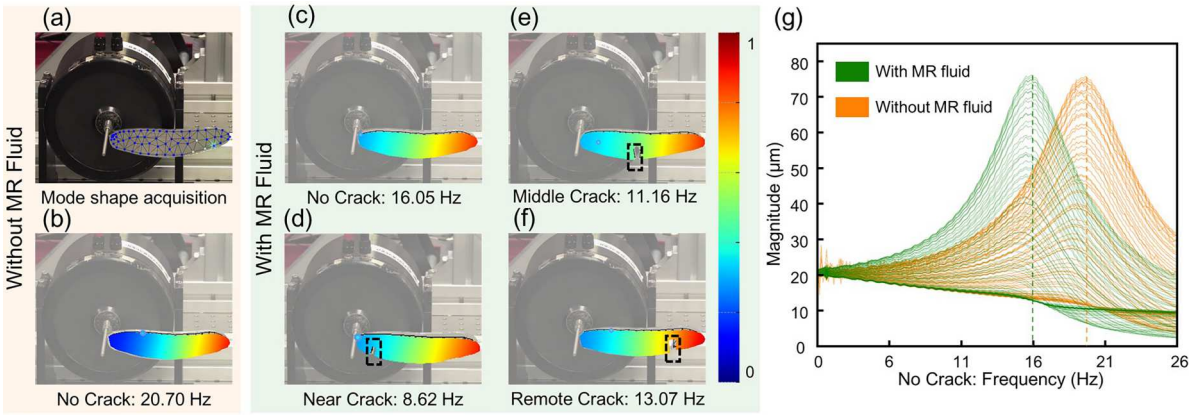


**Figure 2.** Out-of-plane mode shapes of the metamaterial device under different structural configurations. (a) Polytec LDV test setup showing scanning grid. (b) First dominant mode shape of an intact structure without MRF. (c) Mode shape of an intact structure with MRF. (d-f) Mode shapes of cracked structures with MRF, with cracks located near the root, at middle, and at the remote tip, respectively. All modes correspond to the first dominant modal frequency in each case. (g) Comparison of responses at different frequencies for intact structures with and without MRF.

vacuum-assisted injection process. The selected MRF consisted of $Fe_3O_4$ nanoparticles (1-5 μm in diameter) uniformly suspended in a synthetic hydrocarbon carrier fluid, with a saturation magnetisation of approximately 400 mT and a base viscosity below 0.1 Pa·s at zero field. This formulation ensures low flow resistance and rapid magnetic responsiveness. Magnetic field values reported in this study refer to the applied magnetics flux density $B$ (in mT), measured in the specimen region. The corresponding magnetic field strength $H$ can be obtained by $B = \mu_0 H$, where $\mu_0$ is the permeability of free space.

To prevent leakage and maintain long-term stability, all microchannel inlets are sealed with the same photocurable resin and cured at room temperature for 10 h. This encapsulation strategy preserves the mechanical integrity of the structural frame while maintaining channel functionality. As illustrated in Figure 1d, the rigid outer frame provides load-bearing capacity, while the interior lattice beams serve as the integrated modulation zone containing uniformly distributed channels. This configuration allows homogeneous MRF filling and facilitates consistent particle chain formation in response to external magnetic fields. The internal lattice design is further optimised to balance structural stiffness with weight reduction, ensuring sufficient load-bearing capacity without excessive material usage.

A wing-based structural coordinate system is defined as follows: the X-axis runs along the wing plan in the spanwise direction, extending from the wing root to tip. The Y-axis points out of the wing plan, normal to the wing surface, corresponding to transverse deformation. And the Z-axis lies within the wing plan in the chordwise direction, oriented from the leading edge to the trailing edge. Field-induced performance modulation of the metamaterial device is achieved by applying a magnetic field out of the wing plan (Y-axis), as shown in Figure 1e. This orientation promotes optimal alignment of magnetic particles within the embedded channels. Under magnetic activation, the MRF (Figure 1f), a suspension of magnetic particles, forms chain-like structures along the field direction. These particle chains locally reinforce the structure, enabling reversible and spatially programmable modulation of mechanical stiffness. The magnetic field was supplied by a DC electromagnet with a minimum stepping resolution of 0.1 mT, enabling continuous adjustment over the 0–30 mT range. The response time of the magnetorheological fluid to field switching was measured to be <0.5 s. Although the present work employed uniform fields, the same actuation strategy can be extended to segmented coils or programmed gradients, allowing localised and addressable control. This spatiotemporal tunability indicates that the proposed design is compatible with scalable integration into intelligent structures and advanced printing systems.

## 3. Results and discussion

### 3.1. Experimental modal analysis of metamaterial device

The dynamic performance of the metamaterial device is determined not only by its global geometric configuration but also by local stiffness changes induced by structural defects such as cracks [48]. Due to its bioinspired spatial partitioning, embedded microchannel architecture, and non-uniform stiffness distribution, we

conduct non-destructive modal testing to establish a reference basis for subsequent magnetically modulated investigations. Modal characterisation serves to explain the role of internal stiffness gradients in shaping vibrational modes and provides a systematic evaluation of the structure's response under zero-field conditions.

Six representative structural configurations are examined, including an intact sample and three cracked variants with damage localised near, at the middle, and at the remote tip from the root, respectively. To simulate representative failure scenarios, artificial cracks were introduced by precisely cutting through one side of the microchannel walls. Each crack penetrates the full thickness of the beam wall out of the wing plan (Y-axis), with dimensions of approximately 3 mm in width and 10 mm in length. This setup ensures controlled damage severity and location, enabling consistent comparison of modal responses across different defect configurations. As shown in Figure 2a, these structures are tested using a Laser Doppler Vibrometer (LDV, PSV-500)) under two conditions: without with the MRF filling in the absence of external magnetic field. To ensure consistent interpretation and comparability, only the first dominant mode is analysed.

As shown in Figure 2b, the intact structure without the MRF displays a typical cantilever mode shape, characterised by smooth and continuous deformation with the maximum amplitude located at the free end, and the highest vibration amplitude occurs at 20.70 Hz. After infusing the MRF into the internal channels in Figure 2c, the overall vibration amplitude decreases significantly, from 20.70 Hz to 16.05 Hz, and the deformation becomes more localised near the root. This change is attributed to the added mass and the inherent viscosity of the MRF, which increases local inertia and introduce internal damping. In this passive state without magnetic activation, the suspended particles remain randomly dispersed and cannot reinforce the lattice, so the observed frequency downshift is consistently interpreted as a reduction in effective modal stiffness arising from added inertia and viscous damping. Even without magnetic activation, the presence of the MRF passively alters the distribution of modal energy and reduces the structure's dynamic responsiveness.

In Figure 2d-f, introducing cracks at different locations reduces the effective stiffness and leads to measurable shifts in the first-mode resonance frequency, while the overall bending-dominated mode shape is retained. Local deformation amplitudes become uneven across the lattice, reflecting the influence of crack position on stiffness distribution. When the crack is located near the clamped root (Figure 2d), the first natural frequency drops to 8.62 Hz, accompanied by a suppression of vibration amplitude in the damaged region, indicating substantial local stiffness changes. In contrast, cracks positioned at the mid-span (Figure 2e, 11.16 Hz) or near the free tip (Figure 2f, 13.07 Hz) induce a redistribution of modal energy, with deformation concentrated in the remaining undamaged segments. These results demonstrate the dominant mode is highly sensitive to the position of local stiffness disruptions, and that changes in mode shape can be used to identify and localise structural damage. The modal alterations induced by structural damage are entirely passive responses, determined by the fixed geometry and intrinsic material properties of the system. Figure 2g illustrates the difference at the first-mode resonance frequency between the intact structure with and without MRF, under zero magnetic field. The presence of the MRF, even without active magnetic actuation, introduces a baseline stiffness decreasing effect within the microchannels.

Therefore, in the absence of external intervention, the structure is unable to adapt its modal response or compensate for localised stiffness loss. Such modal disruptions remain uncorrected, as the structure lacks any mechanism to recover its original modal characteristics. This limitation creates a clear need for externally applied stimuli capable of modulating local stiffness and rebalancing the vibrational field. This limitation highlights the need for mechanisms capable of actively modulating modal characteristics, particularly in the presence of local stiffness disruptions that passive structures cannot accommodate.

### 3.2. Quasi-static stiffness modulation under magnetic field control

To evaluate the capacity of the magnetically active responsive metamaterial device to modulate stiffness without altering its geometric configuration, we conduct a series of quasi-static compression tests on structures embedded with the MRF. As shown in Figure 3a, the experiments are performed under displacement-controlled loading, with samples clamped between rigid aluminum platens of a mechanical testing system. In Figure 3b, the mechanical properties of the MRF can be altered by introducing and withdrawing the magnetic field. When the magnetic field is removed, the fluid behaves like a medium with unrestricted flow, and the MRF can be regarded as an ultra-flexible material (Fig. S1a). Once a magnetic field is applied, the magnetic particles rearrange along the magnetic field direction (Fig. S1b). Compression is

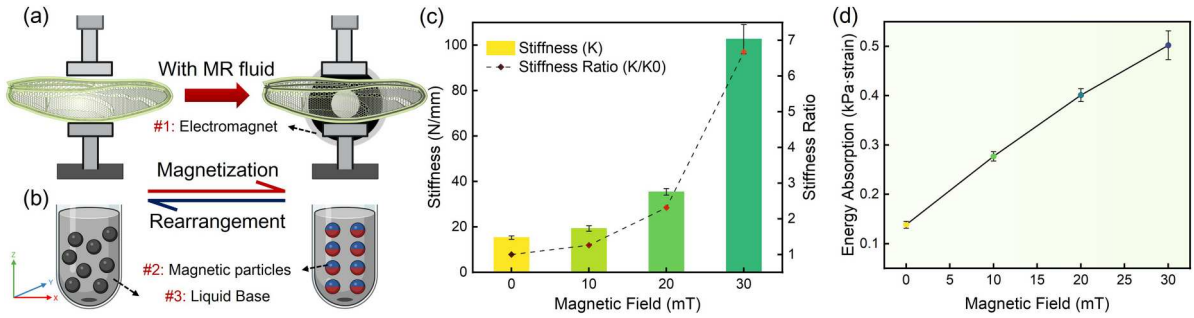


**Figure 3.** Magnetic field-induced stiffness and energy absorption tuning. (a) Compression setup with vertical magnetic actuation enabling the MRF alignment. (b) Distribution within MRF with magnetic field. (c) Stiffness and stiffness ratio increase with field strength (0-30 mT). (d) Energy absorption also increases, demonstrating reversible, field-tunable mechanics.

applied within the wing plan (Z-axis). A vertically oriented electromagnetic coil beneath the specimen generates magnetic fields of 0, 10, 20, and 30 mT, inducing chain formation among magnetic particles within the MRF and thereby introducing anisotropic structural reinforcement.

The quasi-static compression tests demonstrate a clear, monotonic stiffening response under increasing magnetic field strength. As shown in Fig. S2 and Figure 3c, the slope of the force-displacement curve in the elastic regime increases progressively, corresponding to a relative stiffness enhancement of approximately 126% at 10 mT, 231% at 20 mT, and 667% at 30 mT, compared to the zero-field condition. These values are obtained by linear fitting within the initial elastic loading range. In parallel, energy absorption, which is quantified by the area under the stress–strain curve up to 5% strain, is increased by nearly 4 times with field strength (Figure 3d). The simultaneous improvement in both stiffness and energy dissipation reflects a tunable reinforcement effect introduced by magnetic actuation.

Considering the chain-like structure of the MRF, we hypothesise that MRF fillings have a hierarchical structure with lines of magnetic particles parallel to the magnetic field lines, as shown in Fig. S2. The applied strength of the magnetic field not only determines the intensity of the induced magnetisation but also increases the length of the chains of magnetic particles [49]. As particle chains increase in length, uniformly distributed particles are replaced by them (see Fig. S3). During the compression process, longer magnetic lines bend more easily, resulting in a change in deformation mode and greater bending dominance. Therefore, this tunable behaviour arises from the field-induced rheological transition of the MRF. In the absence of a magnetic field, $Fe_3O_4$ nanoparticles are randomly dispersed within the channels and cannot effectively transmit shear loads. However, upon magnetic activation, these particles rapidly align along the field direction to form chain-like microstructures spanning the channel width. These anisotropic chains in turn impose localised constraints on deformation, effectively increasing the local modulus of the microstructured regions. This alters the internal force distribution pathways of the entire lattice in turn, resulting in a substantial enhancement of effective stiffness within the wing plan(Z-axis).

Compared to the conventional strategies based on geometric reconstruction or passively embedded stiffening phases, this approach entails non-contact, reversible, and real-time modulation of mechanical performance via external magnetic fields. Besides, this modulation occurs without altering the structural topology or geometry, preserving design flexibility while expanding the system's functional adaptability. This tunable response under static loading provides a functional basis for dynamic stiffness modulation, allowing the structural properties to be adjusted in a controlled and reversible manner.

### 3.3. Modal response and frequency shift analysis

As an integrated parameter of structural stiffness and mass distribution, modal frequency is highly sensitive to localised stiffness alteration and material state changes [50,51]. It serves as a key dynamic indicator for revealing microstructural reconfiguration effects induced by magnetic actuation. To evaluate the tunability of the metamaterial device's modal characteristics under magnetic fields, experiments are conducted using a harmonic excitation platform. As shown in Figure 4a, the base of the wing is clamped, and a sinusoidal force excitation is applied out of the wing plane (Y-axis). A DC electromagnet positioned beneath the specimen generates magnetic fields of 0, 15, and 30 mT. The response at the wing tip is recorded using a single-point

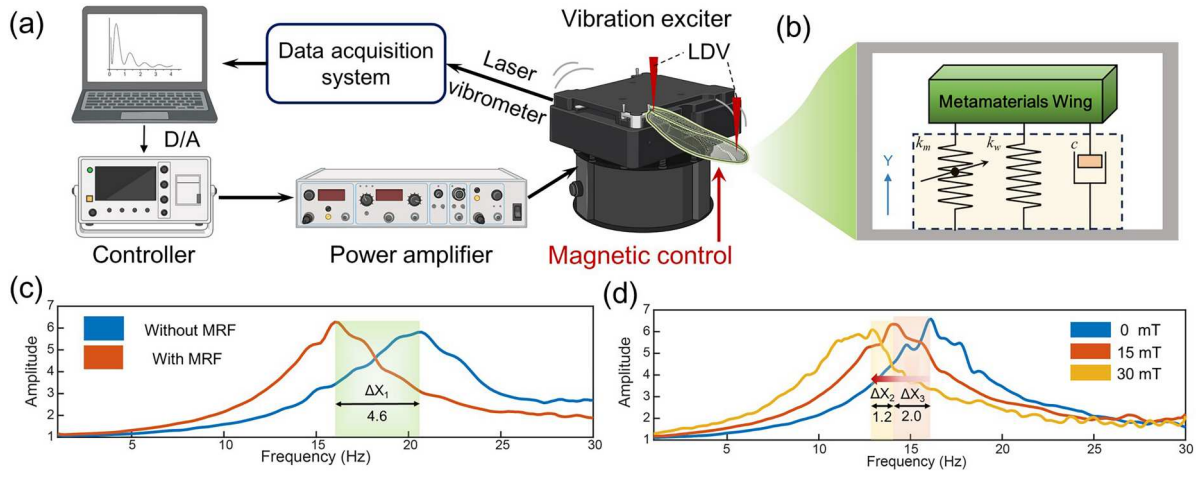


**Figure 4.** Dynamic modal frequency shift under magnetic field actuation. (a) Harmonic excitation setup and data process for frequency response measurement with laser vibrometer. (b) Equivalent mechanical model showing a parallel configuration of intrinsic stiffness $k_w$ and a magnetically tunable negative stiffness element $k_m$, represented as an arrow-headed spring. (c) Comparison of first-mode frequencies with (16.03 Hz) and without MRF (20.63 Hz) under no magnetic field control. (d) Field-dependent response of the MRF-filled structure at 0, 15, and 30 mT, with first-mode frequencies of 16.07, 14.07, and 12.86 Hz, respectively, demonstrating continuous and reversible frequency reduction via field-induced negative stiffness modulation.

LDV, where the frequency response functions (FRFs) are extracted for each field condition. To assess the dynamic performance of the designed metamaterial system, harmonic transmission experiments were performed on the fabricated specimens. A vibration exciter (JZK20) applied a 0-50 Hz linear sweep to one end of the metamaterial device, as illustrated in Figure 4(a). The input sweep signal was generated by a computer, converted by a digital-to-analog interface, and amplified (PA5872) to drive the vibration exciter. The upper excitation displacement $A_{out}(t)$ and the down response $A_{in}(t)$ were recorded simultaneously by two laser vibrometers (KEYENCE LK-G30) with synchronised data acquisition (NI9234). Velocity-displacement records were segmented into time windows (Hann weighting, 50% overlap) and Fourier-transformed to yield amplitude spectra $A_{out}(\omega)$ and $A_{in}(\omega)$. The transmission spectrum was defined as $A_{out}(\omega)/A_{in}(\omega)$. For frequency identification, the first resonance was extracted by peak picking of the dominant spectral maximum. To mitigate spectral broadening and noise bias, a power-weighted centroid ($|A(\omega)|^2$-weighted mean within $\pm 0.5$ Hz of the peak) was also reported. Spectra from three consecutive sweeps were averaged prior to peak picking, by standard random-noise averaging, the RMS of uncorrelated noise scales as $1/\sqrt{N}$ (N = 3), thus improving SNR by approximately $\sqrt{3}$..

To analyse how the magnetic field modulates the first-mode resonance frequency through microstructural changes, an equivalent mass-spring model is established in Figure 4b. Under the assumption of a lightly damped linear oscillator, the system can be idealised as an oscillator comprising an effective stiffness $k_{eff}$ and an effective mass $m$, yielding the natural frequency $f$:

$$f = \frac{1}{2\pi}\sqrt{\frac{k_{eff}}{m}}, \tag{1}$$

$$k_{eff} = k_w + k_m,\ k_m < 0, \tag{2}$$

where $k_w$ is the baseline stiffness of the wing skeleton, and $k_m$ varies with field strength and particle alignment. When the MRF is magnetically activated, the aligned nanoparticle chains introduce a tunable negative stiffness contribution $k_m < 0$. These field-responsive chains are considered as parallel elastic elements, yielding the total effective stiffness. The arrow-headed spring in Figure 4b symbolises this adaptive stiffness component.

In Figure 4c, we compare the first-mode resonance frequencies of the structures with and without MRF filling under zero magnetic field. Quantitatively, the first-mode frequency decreases from 20.63 Hz in the unfilled case to 16.03 Hz after MRF infusion, corresponding to a −22.3% shift. A slight decrease in the resonance frequency is observed upon MRF infusion under zero magnetic field, which is consistent with the passive modal compression effect identified in the previous mode shape analysis discussed in Sec.3.1. Unlike the within the wing plan static loading where the MRF enhances stiffness, the randomly dispersed $Fe_3O_4$ particles cannot contribute to stiffness increase out of the wing plan, which is the direction of dynamic excitation. While the introduction of MRF alters the local material composition and increases the internal mass, the $Fe_3O_4$

nanoparticles remain randomly dispersed without contributing to stiffness enhancement out of the wing plan. Instead, the MRF passively alters the dynamic response by increasing the local inertia within the microchannels, and introducing shear damping through its intrinsic viscosity. These effects reduce the effective dynamic stiffness of the system, causing a measurable downward shift in the resonance frequency.

Figure 4d presents the first-mode frequency response of the MRF-filled structure under increasing magnetic field strengths, the resonance frequency exhibits a downward trend with increasing field intensity. With increasing field, the first-mode resonance shifts from 16.07 Hz (0 mT) to 14.07 Hz (15 mT, – 12.5%) and 12.86 Hz (30 mT, – 20.0%). The average tuning sensitivity is approximately 0.107 Hz/mT across 0–30 mT. Supplementary Video S2 visualises the mode, showing that the bending-dominated shape is retained while the resonance frequency is continuously lowered. Under the magnetic activation, the suspended nanoparticles form chain-like structures aligned along the field lines, producing stable localised reinforcement. These chains reduce their dynamic participation in modal deformation, effectively lowering the contribution of reinforced zones to the global modal stiffness. As a result, the system experiences a continuous reduction in effective modal stiffness, leading to a field-dependent frequency shift. This field-dependent stiffness reduction can be modelled by introducing a magnetically tunable negative stiffness component. Following the mechanical design strategy of quasi-zero-stiffness isolators [52], in which negative stiffness elements enable broadband attenuation through parallel integration with elastic supports, the present magnetic chains can be treated as a field-responsive negative stiffness element $k_m < 0$ in parallel with the original stiffness $k_m$. Thus, in the active state under magnetic field, the frequency downshift is also interpreted as a reduction of effective modal stiffness, here originating from stiffness redistribution rather than additional mass.

For small oscillation amplitudes, this frequency reduction follows the standard linear oscillator model. However, to capture the nonlinear nature of magnetic stiffness modulation, a Duffing-type correction can be introduced to explain the stiffness formulation:

$$k(y) = k_w + k_m + \gamma y^2, \tag{3}$$

where $\gamma$ is the nonlinear stiffness coefficient and $y$ is the local deformation amplitude. The effective stiffness of the system is expressed as $k_{eff}$, where $k_w$ is the baseline wing stiffness and $k_m$ is the magnetically tunable stiffness contribution. This model accounts for the amplitude-dependent stiffness enhancement induced by magnetic chain alignment under increasing strain near damaged regions.

In addition, the field-induced frequency recovery can be estimated quantitatively using the following expression:

$$\Delta f = \frac{1}{2\pi}\left(\sqrt{\frac{K_0 + \Delta K + \Delta K_{mag}}{m}} - \sqrt{\frac{K_0 + \Delta K}{m}}\right), \tag{4}$$

where stiffness reductions (e.g. due to cracks) are represented as negative increments $\Delta K < 0$, and also includes the stiffness increment achieved via magnetic tuning ($\Delta K_{mag} < 0$). Here, $K_0$ denotes the baseline stiffness of the intact structure prior to any damage. This equation offers a direct physical explanation for the experimentally observed frequency shifts $\Delta X_2$ and $\Delta X_3$ upon magnetic field activation. This framework demonstrates that magnetic field-induced structural transformations enable continuously tunable modal frequencies without altering boundary conditions or geometric configuration. The approach constitutes a non-contact, reversible, and programmable dynamic tuning strategy driven by externally actuated negative stiffness modulation.

### 3.4. Crack-induced modal perturbation and damage localisation

As a common form of structural degradation, cracks can significantly affect modal frequencies, mode shapes, and the spatial distribution of vibrational energy [53]. To evaluate the metamaterial device's dynamic adaptability under localised damage conditions, we introduce artificial cracks at representative stress-prone regions to simulate three typical failure scenarios. This analysis assesses whether the proposed system can actively maintain or recover its modal performance in the presence of structural damage, thereby demonstrating its potential for damage-adaptive vibration control.

To model the influence of crack-induced stiffness degradation on modal behaviour, we adopt the analytical framework of a cracked cantilever beam. The free vibration of an intact beam is governed by the Euler-Bernoulli equation:

$$\frac{\partial^4 y(x,t)}{\partial x^4} + \frac{\rho A}{EI}\frac{\partial^2 y(x,t)}{\partial t^2} = 0, \tag{5}$$

where $y(x, t)$ is the transverse displacement, $\rho$ is the density, $A$ is the cross-sectional area, and $EI$ is the flexural rigidity. When a crack is introduced, the structure exhibits a local discontinuity in rotation. The governing

dimensionless vibration equation becomes:

$$\frac{d^4y(\beta)}{d\beta^4} + \lambda^4 y(\beta) = 0,\ \lambda^4 = \frac{\omega^2 \rho A L^4}{EI}. \tag{6}$$

Here, $x$ represents the spatial coordinate along the beam's longitudinal axis, with $x = 0$ at the fixed end of the cantilever beam and $x = L$ at the free end. The beam is modelled as a uniform Euler-Bernoulli cantilever, and the transverse displacement $y\ (x,\ t)$ describes the out-of-plane vibration response over time $t$. $\beta = \frac{x}{L}$ is the dimensionless position coordinate, equivalent to the relative crack location along the beam, and $\omega$ is the angular frequency. At the crack location, a jump in slope is modelled by:

$$y_1' + \lambda \hat{K}_r (y_1'' - y_2'') = 0,\ \hat{K}_r = \frac{K_r L}{EI}, \tag{7}$$

where $K_r$ represents the equivalent rotational stiffness at the crack site. A smaller $K_r$ signifies more severe damage, leading to a reduced effective stiffness and lower eigenfrequencies. The corresponding mode shapes for the beam sections on either side of the crack can be expressed as:

$$y_1 = C_1 \sin(\lambda\beta) + C_2 \cos(\lambda\beta) + C_3 \sinh(\lambda\beta) + C_4 \cosh(\lambda\beta), \tag{8}$$

$$y_2 = C_5 \sin(\lambda\beta) + C_6 \cos(\lambda\beta) + C_7 \sinh(\lambda\beta) + C_8 \cosh(\lambda\beta). \tag{9}$$

Equation (8) and Equation (9) reflect the influence of the stiffness asymmetry across the damaged region. Here, $C_1$ to $C_8$ are the unknown coefficients to be determined by boundary and continuity conditions across the crack interface. As the effective crack stiffness $K_r$ increases due to the field-induced microstructural reinforcement, the discontinuity diminishes, and the frequency partially recovers. A simplified relation between the damaged and the intact modal frequency can be expressed as:

$$\omega_{damaged} = \omega_0 \cdot \sqrt{1 - \alpha},\ \alpha \propto \frac{\Delta K}{K_0}. \tag{10}$$

This model captures the inverse correlation between the local stiffness degradation and the modal frequency. In our system, magnetic actuation reversibly modulates $K_r$, thereby encoding a frequency-restoration mechanism against structural defects.

In Figure 5a, artificial cracks are introduced at three representative locations as before: at the near (i), at the middle (ii), and at the remote tip (iii) of the structure. Each crack penetrated the thickness of a single-side microchannel out of the wing plan, representing typical sites of stress concentration. Under zero magnetic field in Figure 5b, compared to the middle crack, the near crack produces a lower frequency, resulting in a frequency drop defined as $\Delta X_4 = 2.7$ Hz, accompanied by concentrated deformation near the clamped boundary. This reflects local softening and modal energy localisation near the damage site. In contrast, the remote crack results in a frequency increase relative to the middle crack, denoted as $\Delta X_5 = 1.8$ Hz, with the mode shape shifting away from the crack zone, producing an asymmetric vibrational pattern. These results demonstrate that modal behaviour is highly sensitive to the location of stiffness loss, with the spatial distribution of vibrational energy closely following the path and severity of local damage, qualitatively consistent with aforementioned experimental observations.

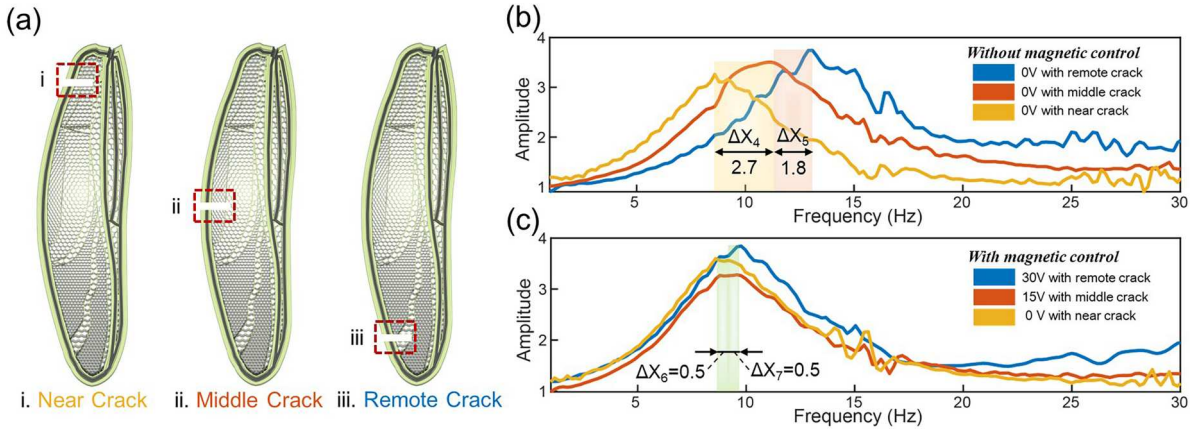


**Figure 5.** Crack-induced modal perturbation and field-mediated compensation. (a) Schematic of artificial cracks at three positions: near, middle, and remote edge. (b) Frequency response comparison of cracked structures under zero field, showing frequency downshifts and modal redistribution. (c) Frequency recovery under applied magnetic fields (15 and 30 mT), indicating partial compensation of stiffness loss through magnetic reinforcement near the damage site.

By controlling the magnetic field, the structure exhibits a field-dependent restoration of modal behaviour, even in the presence of crack-induced stiffness degradation. As shown in Figure 5c, the frequency difference between the root and middle crack cases diminishes as $\Delta X_6 = 0.5$ Hz, while the remote crack frequency converges toward the middle case as $\Delta X_7 = 0.5$ Hz. These observations demonstrate an active compensation mechanism, wherein magnetic field-aligned $Fe_3O_4$ chains locally enhance stiffness near the damaged zones.

To enable quantitative comparison across different crack positions, we further introduce a normalised recovery ratio $R_f$, defined as

$$R_f(B) = \frac{f_{damage,0} - f_{damage,B}}{f_{\text{intact},0} - f_{damage,0}} \tag{11}$$

where $f_{\text{intact},0}$ is the intact zero-field frequency, $f_{\text{damage},0}$ is the damaged zero-field frequency, and $f_{\text{damage},B}$ is the damaged frequency under field $B$. This metric scales from $R_f = 0$ (no recovery) to $R_f = 1$ (full recovery to the intact baseline) and allows different crack severities to be compared on a common basis. Near-root cracks exhibit minimal recovery $R_f \approx 0.005$, mid-span cracks achieve moderate recovery $R_f \approx 0.455$, while tip cracks reach higher recovery $R_f \approx 0.723$, indicating stronger compensation in regions that contribute less to modal curvature. By embedding MRF channels along regions of high modal curvature, field-induced particle chains preferentially bridge cracks and redistribute stiffness where modal sensitivity is greatest, while preserving low-participation regions that enable an effective reduction of modal stiffness and the associated frequency downshift. In contrast, a uniform lattice of comparable mass or porosity would distribute chains more evenly, leading primarily to global stiffening, higher actuation thresholds, and diminished direction selectivity. This is consistent with prior studies showing that asymmetric lattice topologies can access broader and distinct property spaces, such as wider Poisson-ratio ranges and larger shear stiffness-compared with symmetric counterparts. And investigations of disordered metamaterials have revealed that local geometric irregularity can even outperform ordered lattices, breaking conventional strength-toughness trade-offs [54]. In addition, bio-inspired irregular architected materials have been demonstrated to realise spatially varying effective properties that precisely modulate local stress distributions, underscoring the functional role of non-periodicity in enabling localised control [55].

From the modelling perspective, a surface-breaking crack introduces a localised compliance that reduces the effective bending stiffness. This can be interpreted as introducing a local negative stiffness contribution ($k_m < 0$), which lowers the system's modal frequency. When an external magnetic field is applied, suspended magnetic particles align to form chain-like structures that span the cracked regions. These chains restrict deformation and serve as a field-tunable stiffness parameter. The resulting reduction in the local compliance can be modelled as a partial recovery of the negative stiffness magnitude $k_{mag}$, thus decreasing the effective modal stiffness $k_{eff}$. This relationship can be expressed as:

$$k_{eff} = k_w + k_m + \Delta k_{mag}. \tag{12}$$

This mechanism demonstrates that MRF-filled structures not only enable programmable modal tuning under intact conditions but also support adaptive response to localised damage through magnetically actuated compensation. A comparative perspective further clarifies the novelty of this mechanism. As summarised in Supplementary Table S4, prior dragonfly-inspired lattice designs have primarily improved static efficiency, toughness, or passive damping, whereas MRF/MRE-based metamaterials have enabled stiffness tuning, resonant frequency shifts, or tunable bandgaps. However, these approaches have not realised defect-sensitive recovery of modal responses or the preservation of modal coherence under cracks. By combining bio-inspired anisotropy with magnetically reconfigurable mechanics, this present system achieves direction-dependent stiffness tuning together with damage-compensating frequency recovery, thereby addressing a gap unfilled by previous studies. The core principle lies in modulating local stiffness fields via external magnetic stimuli, enabling the system to dynamically reconfigure its modal properties without physical repair. While cracks typically reduce local stiffness and thereby shift the resonance frequencies of the vibration modes, our design leverages field-induced reinforcement of MRF-filled regions to counteract such effects. This compensation restores the first-mode resonance frequency without altering the bending-dominated mode shape, by rebalancing the global stiffness distribution rather than healing material discontinuities. As a result, structurally distinct configurations with different crack locations can be magnetically tuned to exhibit comparable resonance frequencies and consistent modal shapes.

While the current implementation relies on negative stiffness modulation through attraction-dominated magnetic coupling, the underlying principle is equally applicable to positive stiffness control via repulsive interactions. At present, the MRF formulation and electromagnet configuration constrain the response to attraction, future work will explore MRF polarisation

and spatially tailored magnetic fields to enable dual-mode actuation. Such a capability would significantly broaden the design space for programmable stiffness and modal compensation in structurally diverse and damage-prone systems. Potential applications extend to lightweight vibration-damping components in aerospace and robotics, where field-tunable stiffness could support adaptive flight control or soft robotic locomotion. In structural health monitoring, the demonstrated damage-compensating frequency recovery suggests utility for self-healing or fault-tolerant elements requiring preservation of modal integrity under service conditions. Furthermore, the combination of programmable anisotropy and magnetic addressability is inherently compatible with scalable additive manufacturing and 4D-printing technologies, offering pathways toward multifunctional intelligent structures that integrate sensing, actuation, and mechanical adaptation.

## 4. Conclusions

Inspired by the directionally structured mechanics of dragonfly wings, we have demonstrated a bio-inspired tunable metamaterial device that enables direction-dependent stiffness modulation and programmable control over modal properties. Under a magnetic field of 30 mT, the metamaterial device exhibits over 667% enhancement in quasi-static stiffness and 4 times increase in energy absorption in-plane. Meanwhile, dynamic excitation out-of-plane has a reversible reduction in effective modal stiffness in active magnetic control, allowing for contactless frequency tuning. When artificial cracks are introduced, magnetic field induced active tuning can compensate for local stiffness changes, reducing frequency deviation across damaged configurations and restoring stability of modal responses. These results demonstrate a magnetically controlled strategy for adaptive modal tuning and function-level self-healing under structural damage, enabling non-contact, on-demand control of vibrational behaviour without geometric reconfiguration. This capability holds potential for aerospace surface, morphing structures, and intelligent sensing systems that demand resilient and programmable dynamic performance.

## Acknowledgements

This work was supported by the Research Grants Council of the Hong Kong Special Administrative Region, China, under project numbers 11200623 and C7074-23G. This work was also supported by the Teaching Development Grant (Project No. 1085) of The University of Hong Kong and the Global STEM Postdoctoral Research Fellowship (Project No. 2024-0026-013) donated by the Jockey Club Charities Trust. K.G., C.L., Y.N.L., and Y.L. gratefully acknowledge this financial support. The authors also thank the institutional support from the Materials Innovation Institute for Life Sciences and Energy (MILES), the HKU-SIRI platform, and the Consortium for Sound and Vibration Research at The Hong Kong Polytechnic University. Kefan Guo: Conceptualisation, Methodology, Software, Validation, Formal Analysis, Data Curation, Investigation, Writing – Original Draft, Writing – Review & Editing, Visualisation; Chong Li: Conceptualisation, Methodology, Software, Validation, Formal Analysis, Writing – Review & Editing; Chen Gong: Methodology, Validation, Writing – Review & Editing; Yinong Li: Methodology, Software, Validation, Writing – Review & Editing; Li Cheng: Resources, Funding Acquisition, Supervision, Writing – Review & Editing; Yang Lu: Resources, Conceptualisation, Project Administration, Funding Acquisition, Validation, Writing – Review & Editing, Supervision. All authors have read and approved the final version of the manuscript and agree to be accountable for all aspects of the work.

## Author contributions

CRediT: **Kefan Guo:** Conceptualization, Data curation, Formal analysis, Investigation, Methodology, Software, Validation, Visualization, Writing – original draft, Writing – review & editing; **Chong Li:** Conceptualization, Formal analysis, Investigation, Methodology, Software, Validation, Writing – review & editing; **Chen Gong:** Methodology, Validation, Writing – review & editing; **Yinong Li:** Methodology, Software, Validation, Writing – review & editing; **Li Cheng:** Funding acquisition, Resources, Supervision, Writing – review & editing; **Yang Lu:** Conceptualization, Funding acquisition, Methodology, Project administration, Resources, Supervision, Validation, Writing – review & editing.

## Disclosure statement

No potential conflict of interest was reported by the author(s).

## Funding

This work was supported by Teaching Development Grant of The University of Hong Kong: [Grant Number Project No.1085]; Global STEM Post-doctoral Research Fellowship donated by the Jockey Club Charities Trust: [Grant Number 2024-0026-013]; Hong Kong RGC general research fund (No. 11200623, Y. L.) and RGC CRF project (No. C7074-23G, Y. L.).

## Data availability statement

The data that support the findings of this study are available from the corresponding author, Dr. Yang Lu, upon reasonable request, as the dataset forms part of ongoing research projects and further analyses are in progress. The relevant derived data (e.g. summary statistics, figure source data) are available in the manuscript and its supplementary materials. Supplementary Videos are available at: https://doi.org/10.6084/m9.figshare.30111967.

## References


[1] Wang Y, Li L, Hofmann D, et al. Structured fabrics with tunable mechanical properties [J]. Nature. 2021;596:238–243. doi:10.1038/s41586-021-03698-7

[2] Xia X, Afshar A, Yang H, et al. Electrochemically reconfigurable architected materials [J]. Nature. 2019;573:205–213. doi:10.1038/s41586-019-1538-z

[3] Surjadi JU, Gao L, Du H, et al. Mechanical metamaterials and their engineering applications [J]. Adv Eng Mater 2019;21:1800864. doi:10.1002/adem.201800864

[4] Zhang Z, Gao J, Wei S, et al. Lattice-inspired NiTi-based metamaterials with widely tunable mechanical-superelastic synergy [J]. Virtual Phys Prototyp. 2025;20:e2444572. doi:10.1080/17452759.2024.2444572

[5] Yang N, Lin D, Wei H, et al. Mountable lattice metamaterials with In-situ reprogrammable stiffness [J]. Virtual Phys Prototyp. 2025;20:e2499437. doi:10.1080/17452759.2025.2499437

[6] Surjadi JU, Aymon BFG, Carton M, et al. Portela double-network-inspired mechanical metamaterials [J]. Nat Mater. 2025;24:945–954. doi:10.1038/s41563-025-02219-5

[7] Wang Y, Wu K, Zhang X, et al. Superior fracture resistance and topology-induced intrinsic toughening mechanism in 3D shell-based lattice metamaterials [J]. Sci Adv. 2024;10:eadq2664. doi:10.1126/sciadv.adq2664

[8] Bordiga G, Medina E, Jafarzadeh S, et al. Automated discovery of reprogrammable nonlinear dynamic metamaterials [J]. Nat Mater. 2024;23:1486–1494. doi:10.1038/s41563-024-02008-6

[9] Kang Y, Wu L, Tian X, et al. 4D printed thermally tunable metasurface with continuous carbon fibre [J]. Virtual Phys Prototyp. 2023;18:e2224298. doi:10.1080/17452759.2023.2224298

[10] Fang X, Wen J, Cheng L, et al. Programmable gear-based mechanical metamaterials [J]. Nat Mater. 2022;21:869–876. doi:10.1038/s41563-022-01269-3

[11] Ge Q, Li Z, Wang Z, et al. Projection micro stereolithography based 3D printing and its applications [J]. Int J Extreme Manuf. 2020;2:022004. doi:10.1088/2631-7990/ab8d9a

[12] Peng J, Wang S, Liang B, et al. Review of micro and nano scale 3D printing of electromagnetic metamaterial absorbers: mechanism, fabrication, and functionality [J]. Virtual Phys Prototyp. 2024;19:e2378937. doi:10.1080/17452759.2024.2378937

[13] Cheng X, Fan Z, Yao S, et al. Programming 3D curved mesosurfaces using microlattice designs [J]. Science. 2023;379:1225–1232. doi:10.1126/science.adf3824

[14] Li C, Peng Z-K, He Q. Stimuli-responsive metamaterials with information-driven elastodynamics programming [J]. Matter. 2022;5:988–1003. doi:10.1016/j.matt.2021.11.031

[15] Wang C, Chen X, Song Q, et al. Investment micro-casting 3D-printed multi-metamaterial for programmable multimodal biomimetic electronics [J]. Device. 2025;3:100658. doi:10.1016/j.device.2024.100658

[16] Zhao Z, Zhang XS. Encoding reprogrammable properties into magneto-mechanical materials via topology optimization [J]. npj Computational Materials. 2023;9:57. doi:10.1038/s41524-023-00980-2

[17] Zhang W, Chen J, Li X, et al. Liquid metal-polymer microlattice metamaterials with high fracture toughness and damage recoverability [J]. Small. 2020;16:e2004190. doi:10.1002/smll.202004190

[18] Saccone MA, Gallivan RA, Narita K, et al. Additive manufacturing of micro-architected metals via hydrogel infusion [J]. Nature. 2022;612:685–690. doi:10.1038/s41586-022-05433-2

[19] Deshpande VS, Ashby MF, Fleck NA. Foam topology: bending versus stretching dominated architectures [J]. Acta Mater. 2001;49:1035–1040. doi:10.1016/S1359-6454(00)00379-7

[20] Zheng X, Lee H, Weisgraber TH, et al. Ultralight, ultrastiff mechanical metamaterials [J]. Science. 2014;344:1373–1377. doi:10.1126/science.1252291

[21] Jian L, He J, Wen G, et al. Multifunctional TPMS-based metastructures [J]. Int J Mech Sci. 2025;293:110208. doi:10.1016/j.ijmecsci.2025.110208

[22] Al-Ketan O, Abu Al-Rub RK. Multifunctional mechanical metamaterials based on triply periodic minimal surface lattices [J]. Adv Eng Mater. 2019:1900524. doi:10.1002/adem.201900524

[23] Bertoldi K, Vitelli V, Christensen J, et al. Flexible mechanical metamaterials [J]. Nat Rev Mater. 2017:17066. doi:10.1038/natrevmats.2017.66

[24] Rocks JW, Pashine N, Bischofberger I, et al. Designing allostery-inspired response in mechanical networks [J]. Proc Natl Acad Sci U S A. 2017;114:2520–2525. doi:10.1073/pnas.1612139114

[25] Kim T, Hong I, Im S, et al. Wing-strain-based flight control of flapping-wing drones through reinforcement learning [J]. Nature Mach Intell. 2024;6:992–1005. doi:10.1038/s42256-024-00893-9

[26] Zhang S, Sunami Y, Hashimoto H. Deformation behavior of dragonfly-inspired nodus structured wing in gliding flight through experimental visualization approach [J]. Sci Rep. 2018;8:5751. doi:10.1038/s41598-018-24237-x

[27] Gang H, Yang Z, Zhengtong H, et al. Dragonfly-like wing structure enabled by a novel skeleton-reinforced neural style transfer assisted topology optimization and additive manufacturing [J]. Eur J Mech – A/Solids. 2025;112:105631. doi:10.1016/j.euromechsol.2025.105631

[28] He Q, Ferracin S, Raney JR. Programmable responsive metamaterials for mechanical computing and robotics [J]. Nat Comput Sci. 2024;4:567–573. doi:10.1038/s43588-024-00673-w

[29] Liu W, Li F, Liang Y, et al. Three-dimensional double negative mechanical metamaterials with tailored anisotropy [J]. Virtual Phys Prototyp. 2025;20:e2500669. doi:10.1080/17452759.2025.2500669

[30] Dalela S, Balaji PS, Jena DP. A review on application of mechanical metamaterials for vibration control [J]. Mech Adv Mater Struct. 2021;29:3237–3262. doi:10.1080/15376494.2021.1892244

[31] Wei Z, Wang S, Farris S, et al. Towards silent and efficient flight by combining bioinspired owl feather serrations with cicada wing geometry [J]. Nat Commun. 2024;15:4337. doi:10.1038/s41467-024-48454-3

[32] Rader JA, L T. Hedrick morphological evolution of bird wings follows a mechanical sensitivity gradient determined by the aerodynamics of flapping flight [J].

Nat Commun. 2023;14:7494. doi:10.1038/s41467-023-43108-2
[33] Ghavidelnia N, Slesarenko V, Speck O, et al. Bio-Inspired pressure-dependent programmable mechanical metamaterial with self-sealing ability [J]. Adv Mater. 2024;36:e2313125. doi:10.1002/adma.202313125
[34] Wang B, Gao B, Ma B, et al. Bionic programmed wearable actuators based on 4D printing of liquid metal-spidroin-liquid crystal elastomer composite [J]. Virtual Phys Prototyp. 2024;19:e2349677. doi:10.1080/17452759.2024.2349677
[35] Saxena A, Rahn C, Manogharan G. Shape morphing metamaterials via pressure actuated shape morphing cells [J]. Virtual Phys Prototyp. 2025;20:e2468878. doi:10.1080/17452759.2025.2468878
[36] Li C, Jiang T, He Q, et al. Smart metasurface shaft for vibration source identification with a single sensor [J]. J Sound Vib. 2021;493:115836), doi:10.1016/j.jsv.2020.115836
[37] Lu H, Zhang M, Yang Y, et al. A bioinspired multilegged soft millirobot that functions in both dry and wet conditions [J]. Nat Commun. 2018;9:3944. doi:10.1038/s41467-018-06491-9
[38] Li C, Liao X, Peng ZK, et al. Highly sensitive and broadband meta-mechanoreceptor via mechanical frequency-division multiplexing [J]. Nat Commun. 2023;14:5482. doi:10.1038/s41467-023-41222-9
[39] Gong C, Fang X, Cheng L. Band evolution and 2D nonreciprocal wave propagation in strongly nonlinear metaplates [J]. Nonlinear Dyn. 2024;113:1–21.
[40] Xia X, Spadaccini CM, Greer RJ. Responsive materials architected in space and time [J]. Nat Rev Mater. 2022;7:683–701. doi:10.1038/s41578-022-00450-z
[41] Sang L, Wu W, Yao Y, et al. Tuneable mechanical performance and reusability of 4D-printed heterogeneous metamaterials using shape memory biomass-derived polymer [J]. Virtual Phys Prototyp. 2024;19:e2372620. doi:10.1080/17452759.2024.2372620
[42] Cui J, Huang T-Y, Luo Z, et al. Nanomagnetic encoding of shape-morphing micromachines [J]. Nature. 2019;575:164–168. doi:10.1038/s41586-019-1713-2
[43] Ze Q, Kuang X, Wu S, et al. Magnetic shape memory polymers with integrated multifunctional shape manipulation [J]. Adv Mater. 2020;32:e1906657. doi:10.1002/adma.201906657
[44] Zhang W, Zhou J, Jia Y, et al. Magnetoactive microlattice metamaterials with highly tunable stiffness and fast response rate [J]. NPG Asia Mater. 2023;15:45. doi:10.1038/s41427-023-00492-x
[45] Kim Y, Parada GA, Liu S, et al. Ferromagnetic soft continuum robots [J]. Sci Robot. 2019;4:eaax7329. doi:10.1126/scirobotics.aax7329
[46] Kim Y, Yuk H, Zhao R, et al. Printing ferromagnetic domains for untethered fast-transforming soft materials [J]. Nature. 2018;558:274–279. doi:10.1038/s41586-018-0185-0
[47] Zhu Q, Chai K. Magnetic negative stiffness devices for vibration isolation systems: A state-of-the-Art review from theoretical models to engineering applications [J]. Appl Sci. 2024;14:4698. doi:10.3390/app14114698
[48] Pishvar M, Harne RL. Foundations for soft, smart matter by active mechanical metamaterials [J]. Adv Sci (Weinh). 2020;7:2001384.
[49] Wang N, Liu X, Sun S, et al. Microscopic characteristics of magnetorheological fluids subjected to magnetic fields [J]. J Magn Magn Mater. 2020;501:166443. doi:10.1016/j.jmmm.2020.166443
[50] Li C, Jiang T, He Q, et al. Stiffness-mass-coding metamaterial with broadband tunability for low-frequency vibration isolation [J]. J Sound Vib. 2020;489:115685. doi:10.1016/j.jsv.2020.115685
[51] Xu YF, Huang GL. Modal sensitivity analysis of acoustic metamaterials for structural damage detection [J]. Int J Mech Sci. 2023;259:108571), doi:10.1016/j.ijmecsci.2023.108571
[52] Wu J, Zeng L, Han B, et al. Analysis and design of a novel arrayed magnetic spring with high negative stiffness for low-frequency vibration isolation [J]. Int J Mech Sci. 2022;216:106980. doi:10.1016/j.ijmecsci.2021.106980
[53] Gao Z, Zhang X, Wu Y, et al. Damage-programmable design of metamaterials achieving crack-resisting mechanisms seen in nature [J]. Nat Commun. 2024;15:7373. doi:10.1038/s41467-024-51757-0
[54] Srivatsa S, Kumar RS, Selva D, et al. Examining the impact of asymmetry in lattice-based mechanical metamaterials [J]. Mech Mater. 2022;172:104386. doi:10.1016/j.mechmat.2022.104386
[55] Jia Y, Liu K, Zhang XS. Modulate stress distribution with bio-inspired irregular architected materials towards optimal tissue support [J]. Nat Commun. 2024;15:4072. doi:10.1038/s41467-024-47831-2